PROCEEDINGS, Twenty-Eighth Workshop on Geothermal Reservoir Engineering
Stanford University, Stanford, California, January 27-29, 2003
SGP-TR-173

THE ROLE OF SUDDEN DILATIONAL FRACTURING IN EVOLUTION AND MINERALIZATION OF THE SOUTHWESTERN SALTON SEA GEOTHERMAL SYSTEM, IMPERIAL VALLEY, CALIFORNIA

[1]Jeffrey B. Hulen, [2]Denis L. Norton, [1]Joseph N. Moore, [3]William Osborn, [3]Todd van de Putte, and [3]Dennis Kaspereit

[1]Energy & Geoscience Institute, University of Utah, Salt Lake City, UT
[2]Geologist/Geochemist, Stanley, ID
[3]CalEnergy Operating Co., Calipatria, CA

ABSTRACT

Prolific geothermal well Magmamax-6B (M-6B), in the southwestern Salton Sea geothermal field, yields initially 290-298°C hypersaline brine from an interval of hydrothermally altered mudstone and sandstone disrupted by veinlets and breccias mineralized with specular hematite and anhydrite. About half the well's total production is from one such breccia zone that coincides with an abrupt, 8°C reversal in the static-temperature profile.

Converging textural, petrologic, chemical, and thermodynamic evidence suggests that: (1) the M-6B breccias were formed in a strike-slip fault zone as a result of hydraulic implosion abetted by explosion of overpressured, high-temperature pore fluids; (2) the hematite and anhydrite cementing these breccias were precipitated from a downflowing brine originally cooler than the 300°C reservoir rock which the fluid eventually invaded; (3) the downflowing brine may have slightly cooled and mixed with a counterflow of hot brine already ascending the fault zone; (4) the M-6B temperature reversal may be a further consequence of the above process; (5) the reversal nonetheless is only a minor local perturbation in a system that is still thermally prograde; (6) the observed brecciation and mineralization as well as the inferred brine downflow are geologically recent phenomena; (7) sandstones in the reservoir interval are productive only where comparatively shallow and just incipiently altered; and (8) a late-stage assemblage of anhydrite and hematite in this geothermal system may signal favorably rejuvenated porosity and permeability.

Note: Figures follow text

INTRODUCTION

As sole operator of the Salton Sea geothermal field (*Fig. 1*), CalEnergy Corporation has permitted unprecedented (but judicious) access to formerly proprietary borehole samples and resource data. Researchers have accordingly begun to refine and modify classical conceptual models of the field such as those of White et al. (1963), Helgeson (1968), Muffler and White (1969); Elders et al. (1972), Lachenbruch et al. (1985), Elders and Sass (1988), Kasameyer et al. (1988), McKibben et al. (1988), and Williams and McKibben (1989). For example, Hulen and Pulka (2001) and Hulen et al. (2002) have demonstrated (1) that large felsic plutons, rather than mafic ones, are the likely immediate heat sources for this resource; (2) that portions of the field are thermally prograding, rather than cooling and contracting as previously reported for other sectors (e.g., Williams and McKibben, 1989); and (3) that geothermal activity at this site could extend – probably intermittently – back in time a million years or more.

Among the chief practical concerns at this field is the relative contribution to porosity and permeability from fractures and porous sandstones (e.g., Helgeson, 1968; Tewhey, 1977). We have begun to define this relationship utilizing M-6B (*Fig. 2*), one of the most productive wells in the field. The well was completed in 1991 by the former operator, Magma Energy. A full suite of drill cuttings for the well is complemented by a wealth of geophysical-log and reservoir-engineering data.

Results of visual logging, petrographic examination, fluid-inclusion microthermometry, and X-ray diffraction analysis of the cuttings, when compared with corresponding "e-logs" and reservoir measurements in the context of modern geochemical transport theory, provide new insight into this part of the field's complex history and fluid-flow regime. Utilizing this approach, we have (1) determined the proportional contributions of sandstones vs. fractures and breccias to thermal-fluid production; (2) deduced and described the probable processes by which these fractures and breccias were generated; (3) reconciled the modern state and geologically recent evolution of the penetrated hydrothermal system; (4) arrived at a new hypothesis explaining the deep and abundant presence of the assemblage specular hematite-anhydrite in the southwestern SSGF; and (5) reconstructed the past thermal, mechanical, and chemical states of the rocks in which these secondary minerals formed (see also Norton, 1979; and Norton and Dutrow, 2001).

BACKGROUND AND GEOLOGIC SETTING

The SSGF is one of the world's largest developed high-temperature geothermal resources (e.g., Elders and Sass, 1988; Elders, 1989, Hulen et al., 2002), with an installed electrical-generating capacity of 335 megawatts-electrical (MW_e). The field is also in the initial stages of a 185 MW_e expansion –the CalEnergy "Unit 6" development – that will encompass the region surrounding well M-6B (Hulen et al., 2002). A better understanding of reservoir controls in this and existing wells within and near Unit 6 will help enable CalEnergy to develop the expanded resource with optimum efficiency, profitability, and environmental responsibility.

The SSGF is among numerous high-temperature systems scattered throughout the Salton trough (*Fig. 1*), the deeply-sedimented, structural and physiographic northward extension of the Gulf of California (e.g., Elders et al., 1972). The largest and highest-temperature systems (including Mexico's Cerro Prieto) found in the trough to date coincide with spreading centers, or pull-apart basins, formed at the terminations of *en echelon*, right-stepping, right-lateral strike-slip faults separating the North American plate, on the east, with the Pacific plate, on the west. This arrangement of wrench faults and spreading centers links the San Andreas transform, in the northern part of the trough, with the East Pacific rise, at the mouth of the Gulf.

The Salton trough is filled by up to 6 km of fluvial and lacustrine, siliciclastic sediments and sedimentary rocks deposited since about 4 Ma by the Colorado River, when that feature, diverted by a self-constructed alluvial dam across the basin, was flowing northward rather than southward into the Gulf of California (Elders et al., 1972). The developed SSGF is hosted by the upper 1-3 km of this sedimentary sequence. The uppermost layer is mostly semi-consolidated lacustrine mudstone, commonly containing abundant anhydrite (Osborn, 1989). This muddy layer constitutes much of the caprock, or top-seal, inhibiting the escape of heat and fluid from the geothermal system circulating beneath (Helgeson, 1968).

The SSGF is one of only two places in the trough (the other being Cerro Prieto) with exposed Quaternary volcanic rocks. The Salton domes, of late Pleistocene and/or Holocene age (Robinson et al., 1976; Herzig and Elders, 1988) comprise four small rhyolitic extrusive centers aligned northeasterly in the western portion of the field (*Fig. 2*). Hulen et al. (2002) have suggested that the intrusive equivalents of these domes – granitic plutons -- are the likely immediate heat sources for high-temperature hydrothermal activity at this site.
Hot brines are the principal production fluids in the SSGF (e.g.., Helgeson, 1968). The brines are crudely density- and salinity-stratified (McKibben et al., 1988), with total dissolved solids (TDS) values locally as low as 10% toward the surface, and as high as 30% or more at deeper levels. According to Williams and McKibben (1989), mixing of these brines has resulted in widespread precipitation of base-metal sulfides, hematite and other oxides, and diverse secondary silicate phases (see also Helgeson, 1968; McKibben and Hardie, 1997). CalEnergy extracts zinc from the brines using a new method developed exclusively for this resource; the process will ultimately yield about 30,000 metric tons of high-purity zinc *per annum.*

Well M-6B is located in the southwestern portion of the SSGF, where the caprock is thinnest and the top of the convecting geothermal reservoir is closest to the surface (*Fig. 2*). This shallow sector of the resource is elongated

distinctly northeast-southwest, suggesting, in the generally subhorizontal sedimentary sequence here, strong control by faults and fractures. Discussion of the topology of the rest of the SSGF is deferred for a future account.

PRODUCTION WELL M-6B

General – This well is considered to be one of the best and most prolific performers in the SSGF. M-6B yields about 1.2M kg. (2.7M lb.) total mass flow per hour, and even with a relatively small-diameter completion (34 cm, or 13 3/8") supports an electric-power production capacity of about 30 MW_e. For comparison, nearby well Vonderahe-1 has a 40.6 cm (16") completion, yields about 1.6M kg. (3.5M lb.) total mass per hour, and supports a capacity somewhat in excess of 40 MW_e. Vonderahe-1 is the most productive well in the field, but from the foregoing values it seem certain that M-6B would gain the ascendancy if equipped with the larger casing.

Apart from its unusually high productivity, M-6B is a fairly typical well for the southwestern part of the field. The well yields hypersaline brine (~22.3 wt.% TDS) at temperatures near 300°C from relatively shallow depth (only about 1 km). It penetrates the typical Salton trough lithostratigraphic sequence (e.g., Herzig et al., 1988): in essence, an approximately 300 m-thick, evaporite-rich and mudstone-dominated cap above a thick interval of lacustrine and fluvial-deltaic siliciclastic rocks deposited by the Colorado River. Again characteristically, these sediments below about 760 m depth in M-6B are extensively hydrothermally altered and mineralized (further details given below).

Temperatures and Temperature Gradients – Static temperatures measured in M-6B several months after completion define a profile (*Fig. 3*) with four features typical of production wells in this part of the field: (1) a steeply conductive interval, between about 30 m and 360 m depth, corresponding to the impermeable caprock; (2) a hybrid conductive/convective interval between 360 m and about 720 m; and (3) a close-to-isothermal, nearly 300°C leg (720-1200 m) that is interrupted by (4) a small but sharp temperature reversal to a minimum of 290°C at about 1030 m. From the minimum, the temperature climbs gradually to about 294°C at the bottom of the well.

The four thermal zones introduced above stand out even more clearly on a log of thermal gradients with depth (*Fig. 4*). Gradients are commonly >400°C/km in the caprock above about 360 m depth, and in one case approach 1200°C/km. Below the cap, with local exceptions, there is a general trend of decreasing thermal gradients with depth. The temperature reversal zone and immediately underlying interval display sharp fluctuations between notably negative and equally positive gradients, reasons for which remain to be fully understood.

Lost-Circulation Events, Spinner Logs, and Thermal-Fluid Entries – Five lost-circulation events were recorded during the drilling of well M-6B, including a total loss corresponding to the lower 12.2 m (40 ft) of the well (*Fig. 4*). We purposely refer to these losses as "events" rather than "zones", as there is only partial correlation between them and intervals identified as thermal-fluid entries from much more reliable temperature-pressure-spinner (TPS) surveys (*Figs. 3 and 4*). In other words, the losses may have occurred at depths other than the contemporaneous bottom of the borehole. Having said this, however, we note that the lost-circulation events and the spinner-determined fluid entries do both occur below 760 m depth, indicating, if not a one-for-one connection, at least linkage of the two phenomena.

TPS surveys were conducted in M-6B several times after completion of the well in 1991. Fluid-entry zones (*Figs. 3 and 4*) – and their contribution to the total flow -- were interpreted from a composite of these surveys by CalEnergy and Magma Energy reservoir engineers. It is important to note that each of the illustrated and spinner-identified production intervals is an average-inflow zone that was not necessarily matched to a specific geologic feature at the time of the interpretation.

The production brine from M-6B is a composite of the fluids entering the borehole from the five permeable zones identified from TPS surveys. A typical TDS content for this composite brine is 22.3%. Full description of the chemistry of the brine is beyond the scope of this report, but since hematite and anhydrite figure so prominently in our study, it is germane to report that iron in the brine has a typical concentration of 695 ppm; sulfate 105 ppm; and H_2S 11 ppm.

Lithology – Where penetrated by M-6B, the Salton trough sedimentary sequence consists mostly of mudstone (and minor associated argillaceous siltstone), interstratified with lesser amounts of very fine to fine-grained subarkosic sandstone. Where not obviously hydrothermally altered, these sandstones are partially cemented with diagenetic calcite. Their estimated, intrinsic, intergranular porosities fall toward the low end of the 10-30% range reported by Younker et al. (1982) for equivalent rocks in a nearby production well. A few intervals in the uppermost geothermal-reservoir interval (that is, between the base of the cap and about 760 m depth (*Fig. 3*) are more sand than sandstone, with the bulk of the framework grains occurring as single elements, or as clusters of only two or three grains. These sands are relatively quartz-rich and slightly coarser (though still barely medium-grained), and their component grains are commonly rounded and frosted. On this basis, we suspect that the sands are aeolian in origin.

Mudstones account for more than 75% of the total rock volume drilled by M-6B (*Fig. 3*). Where relatively unaltered, the mudstones are calcareous, matte-textured, and range in color from light to medium gray though light to medium grayish-pink, grayish-red, and grayish-orange. A few mudstone intervals host microcrystalline pyrite laminae, probably formed syngenetically through biogenic sulfate reduction (Osborn, 1989). Siltstones are very similar to the mudstones, though seldom accounting for more than a few per cent of the total rock volume. We believe that the mudstones and minor associated argillaceous siltstones are rheologically similar, in orther words, that they probably serve in the sequence as aquicludes unless hydrothermally embrittled and fractured.

Anhydrite occurs sporadically in mudstones and siltstones thoughout the M-6B sequence, but is abundant only in the caprock above a depth of about 360 m (*Fig. 4*). Here, the sulfate occurs principally as ovoid, warty-surfaced nodules up to about a centimeter in maximum dimension. These nodules, with a morphology typical for sabhka depositional environments (Osborn, 1989), range in color from pure white to translucent light gray, the first color confined to microcrytalline varieties, the second to nodules partially to entirely recrystallized to networks of prismatic to tabular anhydrite. A few 6.1 m (20 ft) intervals in the cap consist dominantly of anhydrite, and in these samples the sulfate also occurs as laminated masses that likely formed as lacustrine evaporites. Whether bedded or nodular, the anhydrite of the cap is altered partially to microcrystalline pyrite, again the result of low-temperature, bacteriogenic sulfate reduction (Osborn, 1989). Gypsum accompanies the anhydrite at depths corresponding to temperatures less than the ~100^{o}C dehydration temperature of the mineral.

Below a depth of about 760 m, the mudstones, siltstones, and sandstones are much more indurated than their shallower counterparts, the result of hydrothermal alteration and metamorphism (e.g., Helgeson, 1968; Muffler and White, 1969). These deeper, harder rocks are extensively fractured and veined, and are also locally brecciated or crushed and sheared. Note that veinlets and vein fragments are found only in cuttings samples collected from below a depth of about 800 m (*Fig. 4*). From there to the bottom of the well, however, these veinlets and veinlet fragments typically account for 2-5 vol. % of individual 6.1 m samples, and in one case 9 vol. %. The veinlets record rock rupture and partial hydrothermal sealing of the resulting fractures. Slickensided fault gouge concentrated at about 1070 meters' depth (*Fig. 4*) suggests that many if not all the associated, mineralized fractures (veinlets) are tectonic in origin.

Chips of dilational microbreccia are very common in cuttings collected from below a depth of about 1000 m (*Figs. 4 and 5*). These breccias consist of typically 0.1-1 mm-diameter angular clasts of altered siliciclastic rock arrayed in "jigsaw-puzzle" fashion and cemented, in decreasing order of abundance, by specular hematite, anhydrite, albite, quartz, and chlorite in various combinations. Contacts between cement and clasts are sharp (though crenulated), and cementing minerals typically do not extend into the clasts themselves. The breccias show no sign of crushing and shearing, but clear evidence of volumetric expansion. In this geologic setting, such breccias are most likely to form either by hydrothermal explosion (Grindley and Browne, 1976; Knapp and Knight, 1977) by implosion in dilational jogs along fault zones (e.g., Knapp and Knight, 1977; Sibson, 1986), or, more likely, by a combination of these processes.

Alteration and Mineralization – Whereas rocks in the upper 760 m of well M-6B appear superficially unaltered, rocks below that depth

are extensively altered and mineralized (*Figs. 3-5*). Higher-temperature hydrothermal phases (for example, epidote) become abundant only below about 800 m, coincident with the occurrence of veinlets and veinlet fragments as well as hydrothermally cemented dilational microbreccias. This relationship points to the importance of fractures as the principal means of ingress for the mineralizing hydrothermal fluids.

Based on petrographic observation, intergranular porosity and permeability in sandstone appear to control fluid entries only in the upper part of the M-6B production interval. Just below about 760 m depth (*Fig. 4*), sandstones are only partially altered to (and cemented by) various combinations of quartz, albite, adularia, epidote, chlorite, illite, and traces of base-metal sulfide. These higher-elevation reservoir sandstones, still partially calcite-cemented, retain a significant fraction portion of their original intergranular porosity. By contrast, deeper reservoir sandstones are mostly calcite free and preserve only minor intergranular porosity. The deep sandstones are intensely altered to and cemented by the same secondary minerals noted above but with more epidote as well as minor local actinolite and hematite (*Fig. 4*)

Relatively coarse-crystalline, late-stage specular hematite first appears in cuttings at about 850 m depth, and from there persists to the bottom of the borehole (*Fig. 4*). It occurs in veinlets with anhydrite and lesser albite, quartz, and chlorite, and as a texturally and mineralogically similar cement in dilational microbreccias (*Figs. 5 and 6*). The hematite forms loose clusters of thin, euhedral, bluish-gray metallic scales with bright, translucent, carmine edges. Some of the hematite breccia cements have about 20% intercrystalline porosity, though we cannot be certain that this porosity is interconnected and permeable. Other types of hematitic breccia cement are tightly intergrown with anhydrite (*Fig. 7*).

Crosscutting and infilling textures among secondary minerals encountered in the production interval of M-6B record two distinct stages of mineralization: (1) an earlier stage during which quartz, albite, potassium feldspar (adularia), epidote, actinolite, chlorite, local calcite, base-metal sulfides (pyrite, chalcopyrite, sphalerite, galena), and traces of hematite were precipitated; and (2) a later stage characterized by deposition (with or without quartz) of albite, abundant and coarse-crystalline specular hematite, anhydrite, chlorite, and minor adularia. Contacts between veinlets (and associated wallrock alteration) of the former stage and veinlets and breccia cements of the latter are characteristically sharp and paragenetically unambiguous.

Fluid Inclusions – Anhydrite intergrown with specular hematite in veinlets and breccia cements from the depth range 1170.4-1176.4 m contains abundant fluid inclusions (*Fig. 8*); these were studied to determine the temperatures and salinities of the fluids responsible for deposition of the mineral. The anhydrite contains numerous two-phase (liquid plus vapor), liquid-rich inclusions. Coexisting liquid-rich and vapor-rich inclusions were not observed, suggesting that temperatures during anhydrite deposition were below the boiling point. Many of the inclusions appear to define three-dimensional arrays, one criterion for a primary origin (Roedder, 1984), but could not be related to primary growth features of the host crystals. Homogenization temperatures of 43 of the inclusions ranged from 293°C to 307°C, and averaged 296°C. At such a shallow depth, "pressure corrections" would be trivial for these inclusions, so the stated values are believed to be very close to the true fluid-entrapment temperatures. Ice-melting temperatures of the inclusions ranged from –23.5°C to –24.5°C, and averaged –23.8°C (n=7). The freezing-point depressions of these inclusions indicate fluid salinities of ~25 wt.% NaCl-$CaCl_2$ equivalent. Note that the entrapment temperatures and apparent salinities of these anhydrite-hosted fluid inclusions approximate closely the modern measured temperatures and salinities of brines from the M-6B production zone.

DISCUSSION

Plausible models reconciling the modern thermohydrologic regime and the evolution and mineralization of the geothermal reservoir penetrated by well M-6B must take into account the following measurements, observations and relationships:

- All thermal-fluid production is from reservoir rock that is hydrothermally altered and mineralized, and the bulk of this production is from rock disrupted by either veinlets or dilational breccias,

typically mineralized with specular hematite ± anhydrite.

- The production zones also correlate approximately with more sandstone-rich intervals in the siliciclastic sedimentary sequence hosting the reservoir. However, only in the uppermost (762-808 m) production zone does the sandstone retain significant intergranular porosity. Sandstones of the deeper three zones are tightly cemented by secondary minerals, and would appear to be essentially impermeable unless disrupted by fractures.

- Nearly half the production in well M-6B derives from a major dilational breccia zone characterized by especially intense hematite-anhydrite mineralization. The zone coincides with a minor (from ~298°C to ~290°C) but abrupt temperature reversal in the static temperature profile at about one km depth.

- Homogenization temperatures and apparent salinities for fluid inclusions in anhydrite intergrown with hematite from the dilational breccia zone are essentially identical to modern measured temperatures and salinities for production fluids from these depths.

Origin of the Breccias -- The dilational breccias of the production zone in well M-6B show no indication of crushing, shearing, or granulation, but ample evidence of volumetric expansion. Such breccias, in this environment, can form in only three ways: (1) by high-temperature, explosive natural hydraulic fracturing (Phillips, 1972; Grindley and Browne, 1976; Knapp and Knight, 1977); (2) by implosion along fault zones, particularly at dilational jogs (Sibson, 1986); and (3) by stoping of country rock into volatile-rich pockets within crystallizing magmas, as documented by Sillitoe and Sawkins (1971) and analyzed by Norton and Cathles (1973).

Although there is clear circumstantial evidence of magmatic heat sources for the Salton Sea system, near-field evidence of the requisite large plutons has not been found even in adjacent wells twice as deep as M-6B. Therefore the third brecciation process listed above cannot be regarded as viable here. However, location of the SSGF in one of the world's most seismically active strike-slip fault systems (e.g., Sharp, 1979), coupled with an apparently prograde thermal field in the southwestern SSGF (more discussion below) suggests a more likely composite cause for the brecciation: Lateral displacement along an irregular fault surface augmented by continuously increasing, thermally-driven pore-fluid pressures.

Evolution of the Hydrothermal System – Petrologic, mineralogic, and fluid-inclusion evidence, combined with precise measurement of the temperature and salinity of the modern production brine, permits development of a new geologic and conceptual model for the part of the Salton Sea hydrothermal system penetrated and produced in well M-6B. We believe that the model will apply to much of the entire southwestern part of the SSGF, but proof of this supposition must await the outcome of research still in progress.

The framework for the model (*Fig. 9*) has M-6B intersecting an essentially vertical dilational jog formed along a strike-slip fault of presently conjectural azimuth. Jogs can also develop along normal faults, but are far more common in wrench-fault settings (Sibson, 1985, 1986). On this basis, although we cannot be sure of the fault's displacement from cuttings alone, we feel confident in favoring lateral slip.

According to the model, formation of the jog creates a deeply-penetrating tectonic breccia pipe with dramatically enhanced porosity and permeability. Brecciation is abetted by the extremely high pressures of fluids in isolated pores likely encapsulated along the structure prior to the brecciation event. These pore-fluid pressures build up in response to the prograde thermal field that we argue later in this discussion probably prevails in the southwestern SSGF. Following concepts set forth in Knapp and Knight (1977) and Norton (e.g., 1982, 1984): (1) if the temperature at the depth of the M-6B production zone were, say, 60°C prior to the onset of hydrothermal activity; and (2) if the nominal expansion/compression coefficient of the pore fluids was a thermodynamically reasonable 20 bars/°C, then by the time the rocks at this depth were heated to 300°C, the encapsulated pore fluids would have undergone a 4800-bar fluid-pressure increase. If the initially

sealed fluid packets were suddenly ruptured, they would surely contribute to formation of breccias like those of M-6B.

Extreme depressurization within the breccia pipe would induce the inflow and downflow of brine from surrounding reservoir rock, in a process similar to, but vastly larger in scale than, the one invoked by Moore and Adams (1988) to explain the cementation of nearby shallow sandstones with anhydrite (which has retrograde solubility). One possible scenario involving this process has the brine originating near the base of the cap, and descending while heating in the pipe to the depth of the production zone in well M-6B. Fluid inflow from higher in the cap is possible but conceptually less likely because it seems probable that the plastic, capping muds would quickly seal a fracture even if it had propagated to the surface.

Mineral Metasomatism and Fluid-Rock Interaction -- The downflowing-and- heating brine scenario for the geothermal system encountered by well M-6B can be modeled chemically and thermodynamically utilizing a set of mineral-fluid phase diagrams appropriate for fluids and temperatures theoretically compatible with observed mineral compositions, textures, and paragenetic relationships. The premise for this approach is that the geometric patterns and abundances of secondary minerals produced by hydrothermal activity faithfully record the time-serial history of the causative processes while permitting reconstruction of past thermal, mechanical, and chemical states of the rocks in which the minerals occur (Norton, 1979). At this stage of our investigation, we have focused on simple equilibrium relationships between hydrothermal fluid and the mineral assemblage pyrite-hematite-anhydrite, and on possible processes by which the components of this assemblage may have formed.

As a first step in this exercise, we have generated mineralogical base maps depicting equilibrium amongst minerals and activity ratios of the aqueous components necessary to represent the hydrothermal fluid. These maps, at 200°C and 300°C, provide a basis for discussing hypothetical reaction paths for the descending-and-heating brine scenario introduced above. Constraints for the conservation of mass, energy, and charge were satisfied by basing the analysis on mineral-hydrolysis reactions equating 1 mole of mineral to its aqueous-ion components. Thus:

- Anhydrite: $CaSO_4 = Ca^{+2} + SO_4^{-2}$
- Hematite: $Fe_2O_3 + 3.5H^+ + 0.25H_2S = 2Fe^{+2} + 0.25SO_4^{-2} + 2H_2O$
- Pyrite: $FeS_2 + 1.5H^+ + H_2O = Fe^{+2} + 1.75H_2S + 0.25SO_4^{-2}$

Mapped onto ion-activity diagrams appropriate for 200°C and 300°C, these minerals and the fluid can be discussed in terms of the conceptual fluid-flow model introduced above. Data for these activity diagrams are from the SPRONS.dat thermodynamic database developed by Helgeson (1970; see also Helgeson et al., 1978). The data are based on experimental and theoretical information compiled into an internally consistent set. Because coordinates for the diagrams are constructed from activity ratios, the indicated mineral relationships are independent of bulk chemical variations in the causative hydrothermal fluid.

The common association of quartz with the principal secondary minerals selected for this analysis permits equating Log $a(SiO_2)$ to quartz saturation. Likewise, the common association of epidote in the deeper reaches of M-6B enables Log $[a(Ca^{+2})/a(H^+)]^2$ for the 300°C case to be fixed provisionally at 7, a value appropriate for epidote with $X_{pistacite} = 0.33$. Epidote is unstable at the lower temperature, 200°C, but we assume for the model a copious supply of calcium in fluid, and fix the corresponding Log $[a(Ca^{+2})/a(H^+)]2$ also at a value of 7. Finally, $a(H_2O)$ is assumed to be unity even though it will be clearly be less than this value in the Salton Sea production brines; the essence of this discussion is not significantly affected by the departure.

One hypothetical fluid-reaction path for the downward-flowing, fracture-channeled brine envisioned above is illustrated on *Figure 10*, which combines the activity diagrams constructed for 200°C and 300°C. At the lower temperature, appropriate for the base of the caprock, the fluid is theoretically in equilibrium with the anhydrite and pyrite commonly observed together in the cap's lower half. If we assume arbitrarily that the initial H_2S activity of the descending and heating brine remains constant, then as the brine moves toward the 300°C geothermal reservoir rock at depth, it will first co-precipitate anhydrite and pyrite, then

eventually anhydrite and hematite. The latter equilibrium mineral set is precisely the one observed in the dilational breccias and veinlets of the production zone in well M-6B.

The fact that the production brine matches closely in salinity and temperature corresponding values obtained from fluid inclusions in the anhydrite-hematite breccia cement suggests that the brecciation and mineralization are, geologically speaking, quite recent phenomena. This could help explain the minor temperature reversal at about 1 km depth (*Figs. 3 and 4*). Though becoming ever hotter with depth, the downflowing brine may have arrived in the production zone at just slightly cooler temperatures than the ~300oC that likely initially prevailed before the influx.

Is the Southwestern SSGF Thermally Prograde or Retrograde? – The slight cooling of the production zone in M-6B and other wells in the southwestern SSGF by no means indicates that this part of the system, like (apparently) its more northerly counterpart (e.g., Williams and McKibben, 1988), has waned from its thermal maximum. On the contrary, we believe that the southwestern SSGF could still be vigorously prograde, with only minor local perturbations, like the M-6B temperature reversal, even hinting at the onset of thermal retreat. We hasten to add that these fluctuations occur on a geologic time scale (probably centuries to thousands of years at minimum) that clearly does not impact the robust contemporary productivity of the entire SSGF.

Figure 11 shows a series of temperature-depth profiles through time computed by one of us (Norton) for a simplified, 2D, numerical hydrothermal system broadly similar to the one now active at the SSGF. Modeling methods and assumptions are discussed in Norton (1979, 1982, 1984) and Norton and Taylor (1979), to which the reader is referred for details. These models will be constantly refined as our work on the SSGF progresses, but for now, even the preliminary thermal profiles address the current thermal state of M-6B and probably the entire southwestern part of the geothermal field.

For purposes of this investigation, we highlight a key aspect of the numerical temperature-depth profiles: only as the system is thermally prograding are the profiles concave-upward in the caprock above the convecting portion of the hydrothermal system (that is, where the curves steepen and converge at closer to isothermal values). The profile for well State 2-14 (from Elders and Sass, 1988), in the northern part of the field (*Fig. 1*) suggests that the system there is either at its thermal maximum or has begun to contract and cool (again, over geologic time). It is important to note here that, although not illustrated, the general convex-up configuration exhibited by the thermal-peak profile persists as the numerical system cools. By contrast, from the illustrated thermal profile for well M-6B (*Fig. 11*), it is difficult to imagine a greater thermal peak from which that profile *could* have retreated. Accordingly, we reiterate that the geothermal system penetrated by this well is likely to be near its thermal apex.

SYNOPSIS

Results of our multidisciplinary investigation of production well M-6B lead us to the following conclusions:

- Fractures and breccias are the dominant controls on thermal-fluid flow in the production zone. Sandstones are also productive, but only where comparatively shallow and only weakly altered. Most deeper sandstones are intensely altered, tightly hydrothermally cemented, and only sparingly permeable unless disrupted by fractures and breccias.

- These fractures and breccias formed rapidly under the influence of coupled tectonic and hydrothermal processes. Along a strike-slip fault within a deeply-penetrating dilational jog, the rocks could have ruptured in response to a combination of depressurization-induced implosion and hydrothermal explosion, the latter caused by release of extreme overpressures (relative to hydrostatic) in initially isolated, high-temperature fluid packets.

- Hematite and anhydrite filling the fractures and cementing the breccias were precipitated from a downflowing (and/or inflowing) brine initially at a lower temperature than the ~300^{o}C geothermal reservoir where the fluid eventually arrived.

- The downflowing brine may have slightly cooled (and probably mixed with) a counterflow of hot brine initially ascending in the fault zone. The slight temperature reversal now observed in the production zone may be a further consequence of this process.

- The close match of fluid-inclusion and modern measured temperatures and salinities suggests that brecciation and subsequent anhydrite-hematite mineralization are geologically recent phenomena.

- The temperature reversal in the production zone is a minor local feature in a hydrothermal system at or near its fullest thermal expansion.

- Late-stage hydrothermal hematite and anhydrite appear to signal zones of new or rejuvenated porosity and permeability particularly amenable to commercial thermal-fluid production.

ACKNOWLEDGEMENTS

We thank CalEnergy Operating Company and MidAmerican Energy Holdings for permission to publish these results. Hulen and Norton's participation in this project is sponsored by the Department of Energy, Office of Geothermal Technologies, under Grant No. DE-FG07-00ID13891. The first author is grateful to Fred Pulka for generously sharing his considerable expertise on this resource. Thanks to Melinda Wright for providing valuable information and advice about the thermal regime and chemistry of produced brine from well M-6B. Louise Spann completed X-ray diffraction analyses. Illustrations are the work of graphic artist Doug Jensen.

REFERENCES

Elders, W.A., 1989, Geothermal resource assessment of the Salton Sea geothermal field, California: University of California, Riverside, Report UCR/IGPP/89-32, 4 p.

Elders, W.A., and Sass, J.H., 1988, The Salton Sea scientific drilling project – Its scientific significance: Journal of Geophysical Research, v. 93, p. 12,953-12,968.

Elders, W.A., Rex, R.W., Meidav, T., Robinson, P.T., and Biehler, S., 1972, Crustal spreading in southern California – The Imperial Valley and the Gulf of California formed by rifting apart of a continental plate: Science, v. 178, p. 15-24.

Grindley, G.W., and Browne, P.R.L., 1976, Structural and hydrologic factors controlling the permeability of some hot-water geothermal fields: United Nations Symposium on Development and Use of Geothermal Resources, 2nd, San Francisco, California, 20-29 May, 1975, Proceedings, p. 377-386.

Helgeson, H.C., 1968, Geologic and thermodynamic characteristics of the Salton Sea geothermal system: American Journal of Science, v. 266, p. 129-166.

Helgeson, H.C., 1970, Description and interpretation of phase relations in geochemical processes involving aqueous solutions: American Journal of Science, v. 268, p. 415-438.

Helgeson, H.C., Delaney, J.M., Nesbitt, H.W., and Bird, D.K., 1978, Summary and critique of the thermodynamic properties of rock-forming minerals: American Journal of Science, v. 278A, 229 p.

Herzig, C.T., and Elders, W.A., 1988, Nature and occurrence of igneous rocks cored in the State 2-14 research borehole, Salton Sea Scientific Drilling Project, California: Journal of Geophysical Research, v. 93, p. 13,069-13,080

Herzig, C.T., Mehegan, J.M., and Stelting, C.E., 1988a, Lithostratigraphy of the State 2-14 borehole, Salton Sea Scientific Drilling Project: Journal of Geophysical Research, v. 93, p. 12,969-12,980.

Hulen, J.B., and Pulka, F.S., 2001, Newly-discovered, ancient extrusive rhyolite in the Salton Sea geothermal field,

Imperial Valley, California – Implications for reservoir characterization and duration of volcanism in the Salton trough: Stanford University, 26th Workshop on Geothermal Reservoir Engineering, Proceedings, 10 p.

Hulen, J.B., Kaspereit, D., Norton, D.L., Osborn, W., and Pulka, F.S., Refined conceptual modeling and a new resource estimate for the Salton Sea geothermal field, Imperial Valley, California: Geothermal Resources Council, Transactions, v. 26, p. 29-36.

Kasameyer, P.W., Younker, L.M., and Hanson, J.M., 1988, Development and application of a hydrothermal model for the Salton Sea geothermal field, California: Geological Society of America Bulletin, v. 95, p. 1242-1252.

Knapp, R.B., and Knight, J.E., 1977, Differential thermal expansion of pore fluids – Fracture propagation and microearthquake production in hot pluton environments: Journal of Geophysical Research, v. 82, p. 2515-2522.

Lachenbruch, A.H., Sass, J.H., and Galanis, S.P., Heat flow in southernmost California and the origin of the Salton trough: Journal of Geophysical Research, v. 90, p. 6709-6736.

McKibben, M.A., and Hardie, L.A., 1987, Ore-forming brines in active continental rifts *in* Geochemistry of hydrothermal ore solutions, 3rd edition (H.L. Barnes, ed.): New York, John Wiley, p. 877-935.

McKibben, M.A., Andes, J.P., Jr., and Williams, A., 1988, Active ore formation at a brine interface in metamorphosed deltaic lacustrine sediments – The Salton Sea geothermal system, California: Economic Geology, v. 83, p. 511-523.

Moore, J.N., and Adams, M.C., 1988, Evolution of the thermal cap in two wells from the Salton Sea geothermal system, California: Geothermics, v. 17, p. 695-710.

Muffler, L.J.P., and White, D.E., 1969, Active metamorphism of Upper Cenozoic sediments in the Salton Sea geothermal field and the Salton trough, California: Geological Society of America Bulletin, v. 80, p. 157-182.

Newmark, R.L., Kasameyer, P.W., Younker, L.W., and Lysne, P., 1988, Shallow drilling in the Salton Sea region – The thermal anomaly: Journal of Geophysical Research, v. 93, p. 13,005-13,024.

Norton, D.L., 1979, Transport phenomena in hydrothermal systems – The redistribution of chemical components around cooling magmas: Bulletin de Mineralogie, v. 102, p. 471-486.

Norton, D.L., 1982, Fluid and heat transport phenomena typical of copper-bearing pluton environments *in* Advances in geology of the porphyry copper deposits, southwestern North America (S.R. Titley, ed.): Tucson, University of Arizona Press, p. 59-72.

Norton, D.L., 1984, The theory of hydrothermal systems: Annual Review of Earth and Planetary Sciences, v. 12, p. 155-177.

Norton, D.L., and Cathles, L.M., 1973, Breccia pipes – Products of exsolved vapor from magmas: Economic Geology, v. 68, p. 540-546.

Norton, D.L., and Dutrow, B.L., 2001, Complex behavior of magma-hydrothermal processes – Role of supercritical fluid: Geochimica et Cosmochimica Acta, v. 65, p. 4009-4017.

Norton, D.L., and Taylor, H.P., 1979, Quantitative simulation of the hydrothermal systems of crystallizing magmas on the basis of transport theory and oxygen-isotope data – An analysis of the Skaergaard intrusion: Journal of Petrology, v. 20, p. 421-486.

Osborn, W.L., 1989, Formation, diagenesis, and metamorphism of sulfate minerals in the Salton Sea geothermal system,

California: University of California, Riverside, M.S. Thesis, 175 p.

Robinson, P.T., Elders, W.A., and Muffler, L.J.P., 1976, Quaternary volcanism in the Salton Sea geothermal field, Imperial Valley, California: Geological Society of America Bulletin, v. 87, p. 347-360.

Roedder, E., 1984, Fluid inclusions: Reviews in Mineralogy, v. 12, 644 p.

Rook, S.H., and Williams, G.C., 1942, Imperial carbon dioxide field: California Division of Oil and Gas, Summary of Operations, Oil Fields, July-December 1942, v. 28, p. 12-33.

Sharp, R.V., 1979, Tectonic setting of the Imperial Valley Region *in* The Imperial Valley, California, Earthquake of October 15, 1979: U.S. Geological Survey Professional Paper 1254, p. 5-14.

Sibson, R.H., 1985, Stopping of earthquake ruptures at dilational jogs: Nature, v. 316, p. 248-251.

Sibson, R.H., 1986, Brecciation processes in fault zones – Inferences from earthquake rupturing: Pure and Applied Geophysics, v. 124, p. 159-175.

Sillitoe, R.H., and Sawkins, F.J., 1971, Geologic, mineralogic, and fluid-inclusion studies relating to the origin of copper-bearing tourmaline breccia pipes, Chile: Economic Geology, v. 66, p. 1028-1041.

Tewhey, J.D., 1977, Geologic characteristics of a portion of the Salton Sea geothermal field: Lawrence Livermore Laboratory, Report UCRL-52267, 51 p.

White, D.E., Anderson, E.T., and Grubbs, D.K., 1963, Geothermal brine well – Mile-deep drill hole may tap ore-bearing magmatic waters and rocks undergoing metamorphism: Science, v. 139, p. 919-922.

Williams, A.E., and McKibben, M.A., 1988, A brine interface in the Salton Sea geothermal system, California: Fluid-geochemical and isotopic characteristics: Geochimica et Cosmochimica Acta, v. 53, p. 1905-1920.

Younker, L.W., Kasameyer, P.K., and Tewhey, J.D., 1982, Geological, geophysical, and thermal characteristics of the Salton Sea geothermal field, California: Journal of Volcanology and Geothermal Research, v. 12, p. 221-258.

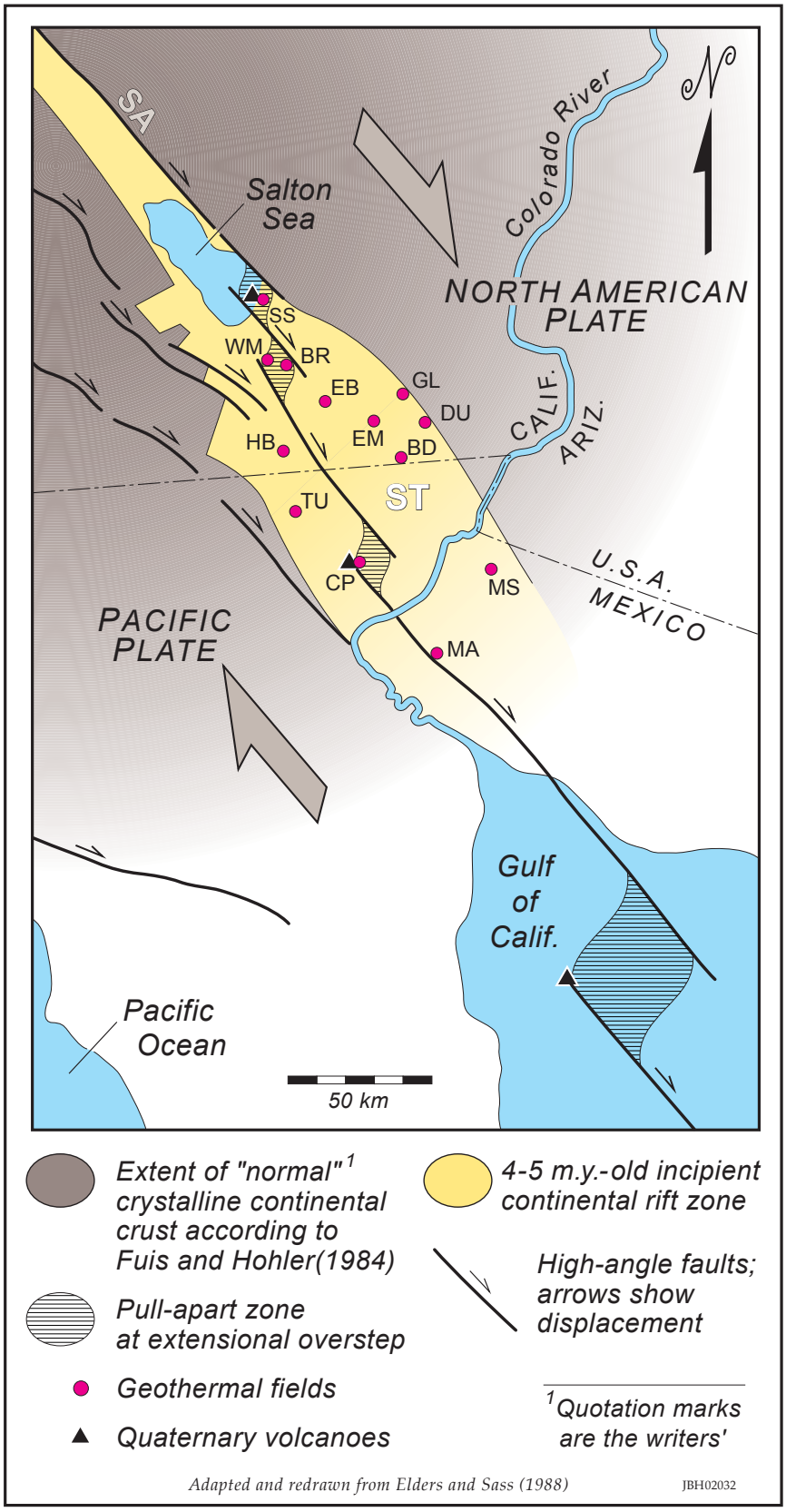

Figure 1. Location and tectonic map of the Salton trough (ST) and its high-temperature geothermal systems relative to the southeastern terminus of the San Andreas transform fault zone (SA) and the tip of the Gulf of California. Geothermal fields (not all currently producing) abbreviated as follows: BD – Border; BR – Brawley; EB – East Brawley; EM – East Mesa; GL – Glamis; HB – Heber; MA – Mesa de Andrade; MS – Mesa de San Luis; SS – Salton Sea; TU – Tulecheck; WM – Westmoreland. Large arrows show modern relative motion of tectonic plates.

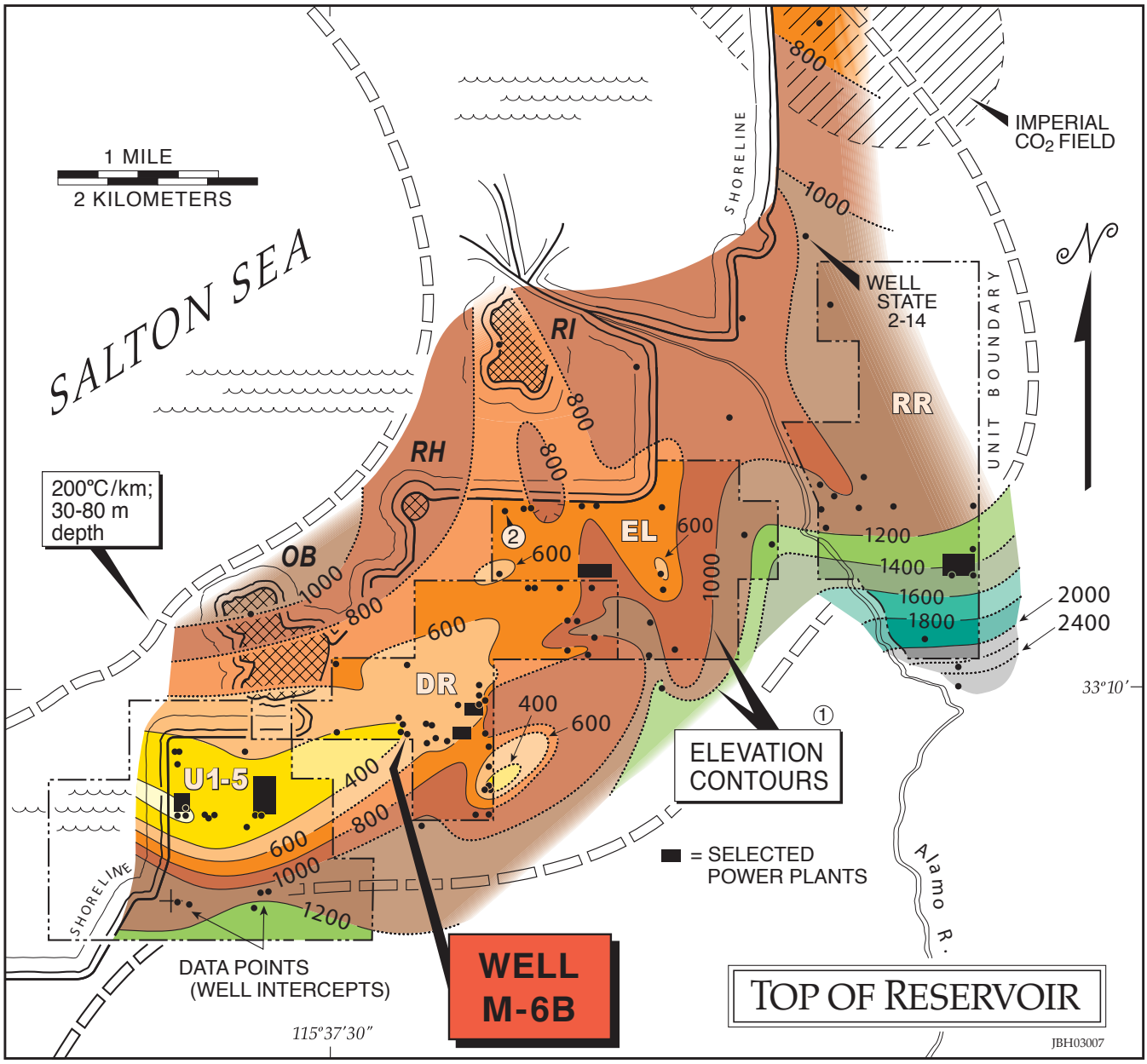

① Meters below mean sea level; dotted where projected between or beyond unit boundaries. ② Well Elmore 1 NOTE: Ground level = (-)69 m

Figure 2. Location of geothermal well M-6B relative to the configuration of the top of the convecting Salton Sea geothermal system. Note that the well is located at the northeastern end of a prominent, northeast-southwest elongated reservoir-top "high." The "high" is oriented subparallel to the ideal trend for an antithetic, left-lateral strike-slip fault in the prevailing, San Andreas-style, right-lateral wrench-fault regime. Cross-hatched areas signify Late Quaternary rhyolitic volcanic centers: OB - Obsidian Butte; RH - Rock Hill; RI - Red Island. A fourth such center, Mullet Island, is located just to the north-northwest of top center of the figure. Additional abbreviations: DR - Del Ranch production unit; EL - Elmore production unit; RR - River Ranch production unit; U1-5 - production units 1 to 5.

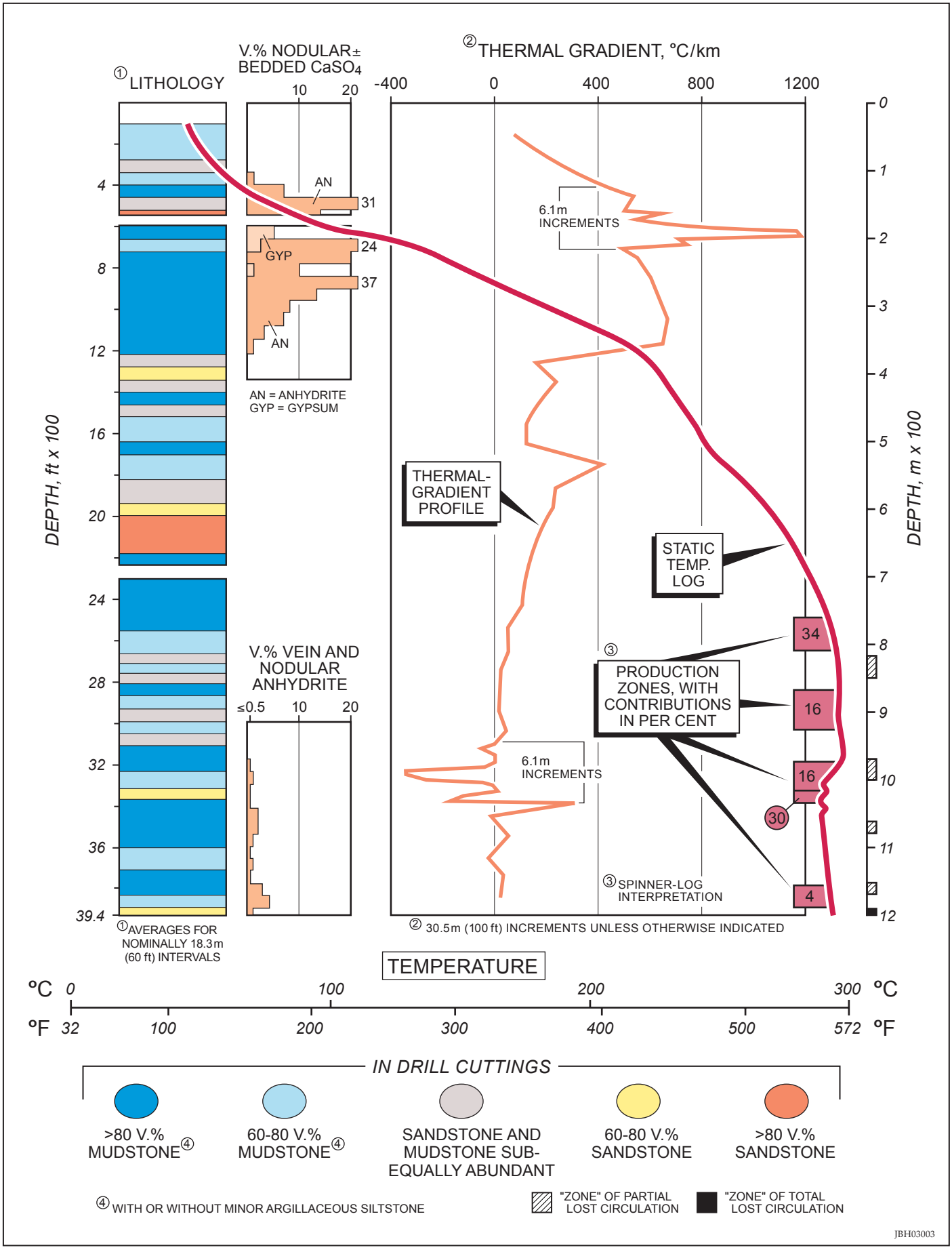

Figure 3. Lithologic, static-temperature, and thermal-gradient logs for well M-6B. Lost-circulation "zones" record only total borehole depth at the time the losses occurred. Please refer to text for further explanation.

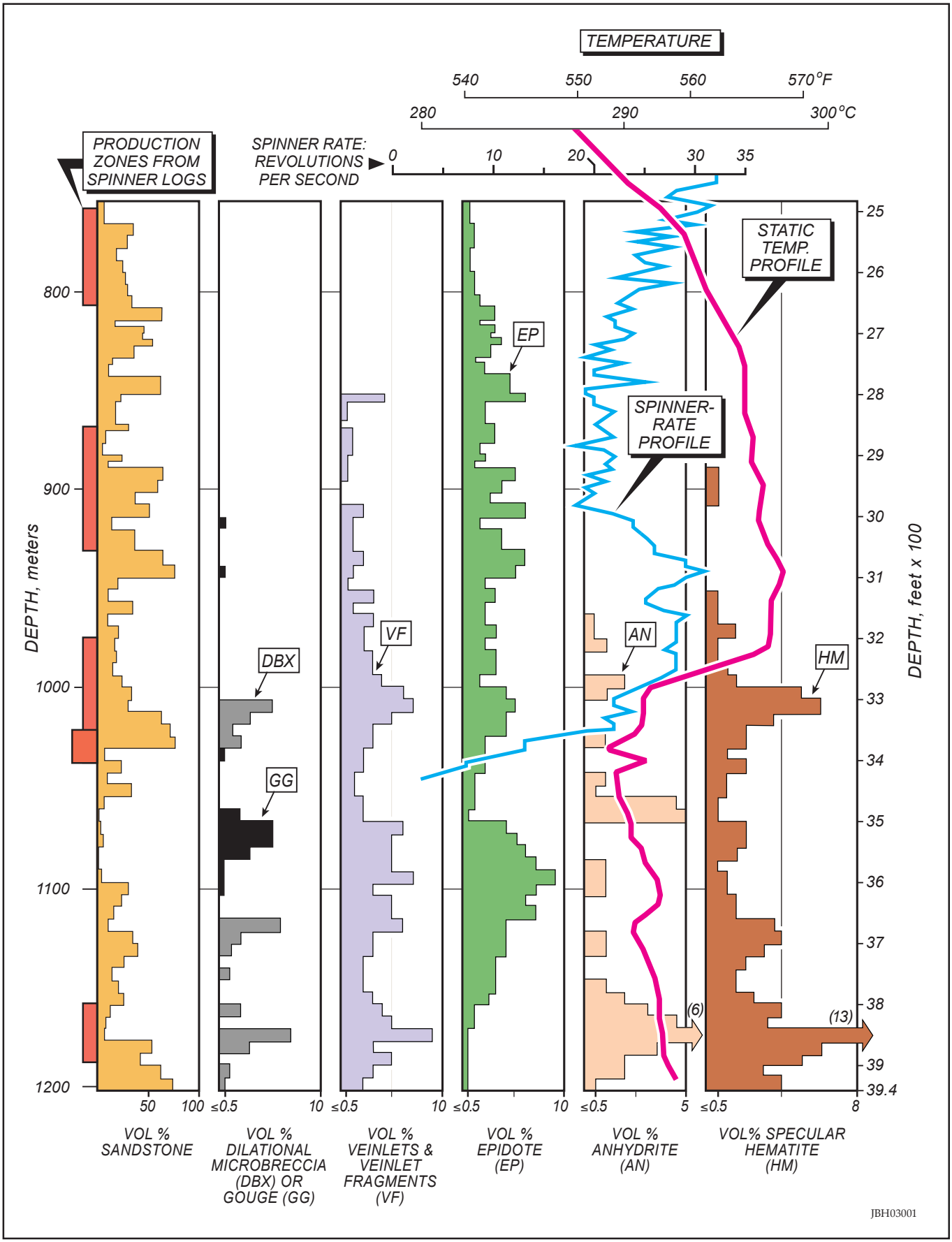

Figure 4. Detailed static-temperature and spinner logs vs the downhole distributions of selected secondary minerals, veinlets and veinlet fragments, gouge, and dilational microbreccia through the production interval in well M-6B. Please note that the spinner-log-determined production zones (see also Figure 3) are "average-inflow" zones determined by reservoir engineers and not necessarily matched to specific geologic features at the time of interpretation. In other words, the actual entries within these zones could be much more restricted in vertical extent.

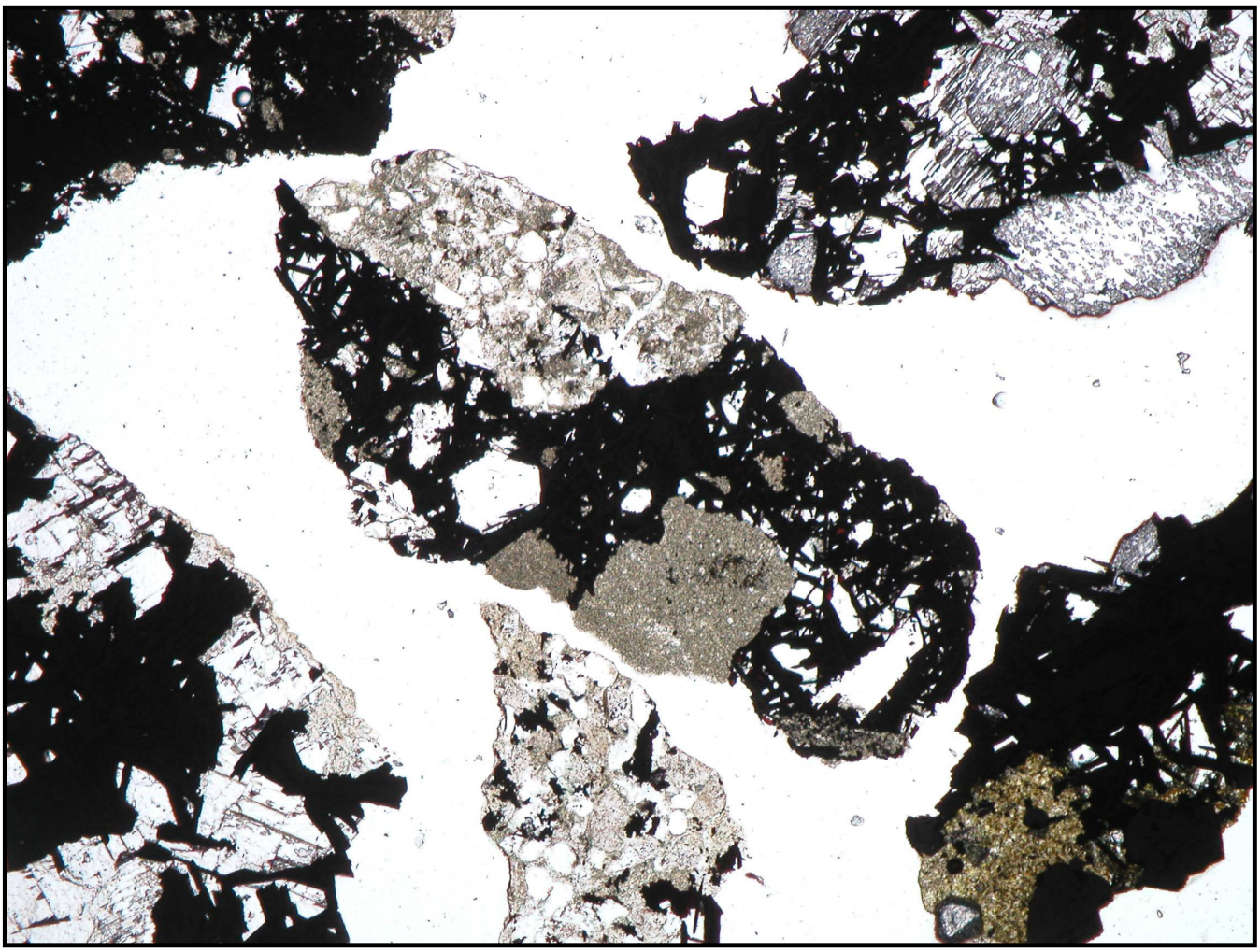

Figure 5. Photomicrograph (plane polarized light) of drill cuttings of hematite-anhydrite-cemented, dilational microbreccia from the interval 1170.4-1176.4 m in well M-6B. Chip in the center of the field of view is ~1 mm long. Black material is specular hematite cement. The hematite is intergrown with anhydrite in the chip at lower left. Clasts comprise hydrothermally altered sandstone, mudstone, and earlier vein quartz.

Figure 6. Photomicrograph (plane polarized light) of part of a drill chip of loosely intergrown specular hematite breccia cement from the interval 1170.4-1176.4 m. Long dimension of field of view ~1.3 mm. Angular white areas are voids.

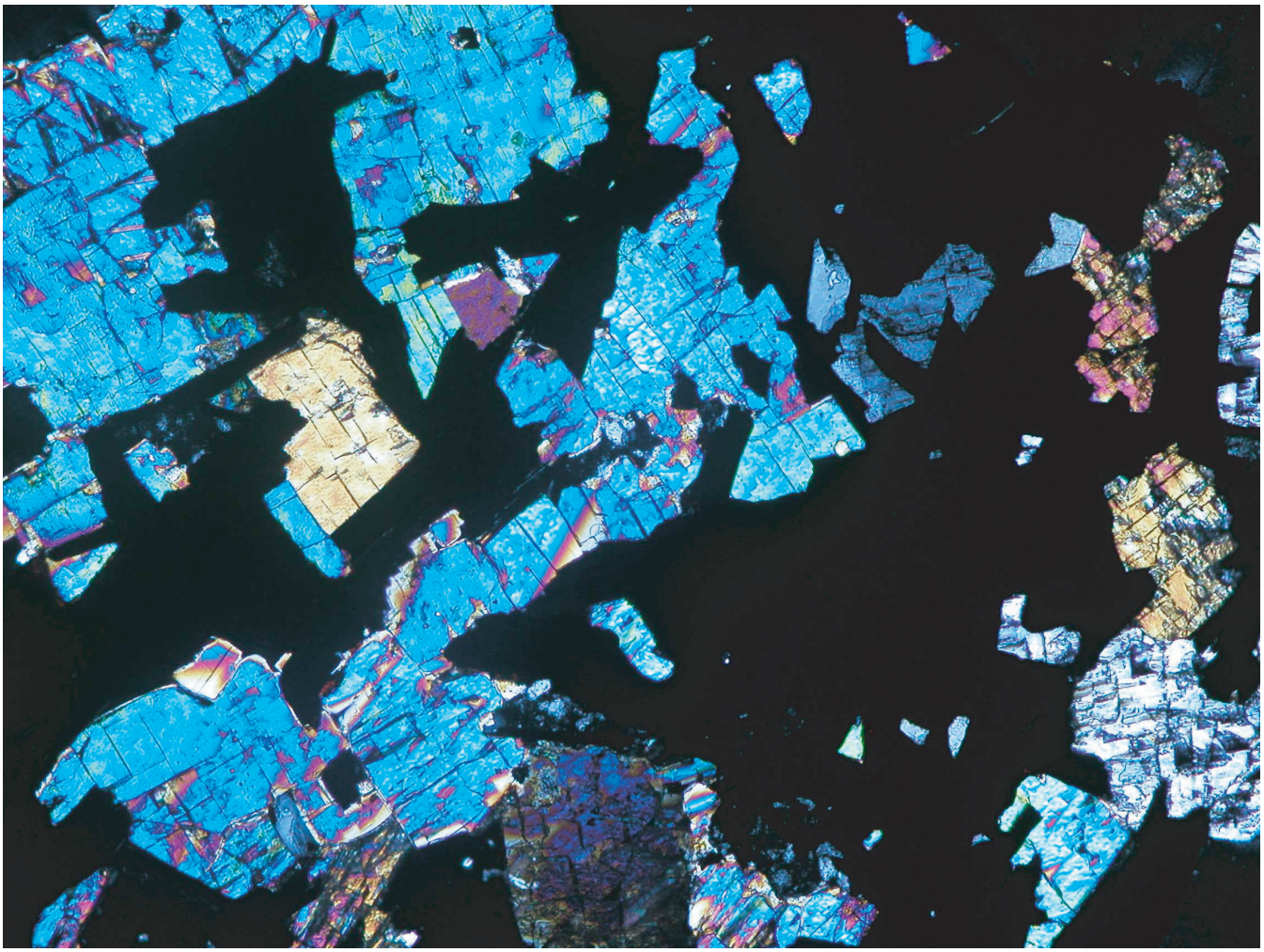

Figure 7. Photomicrograph (crossed nicols) of specular hematite (black) intergrown with anhydrite (brightly colored areas) in dilational breccia cement from the depth interval 1170.4-1176.4 m in well M-6B. Long dimension of field of view ~2mm.

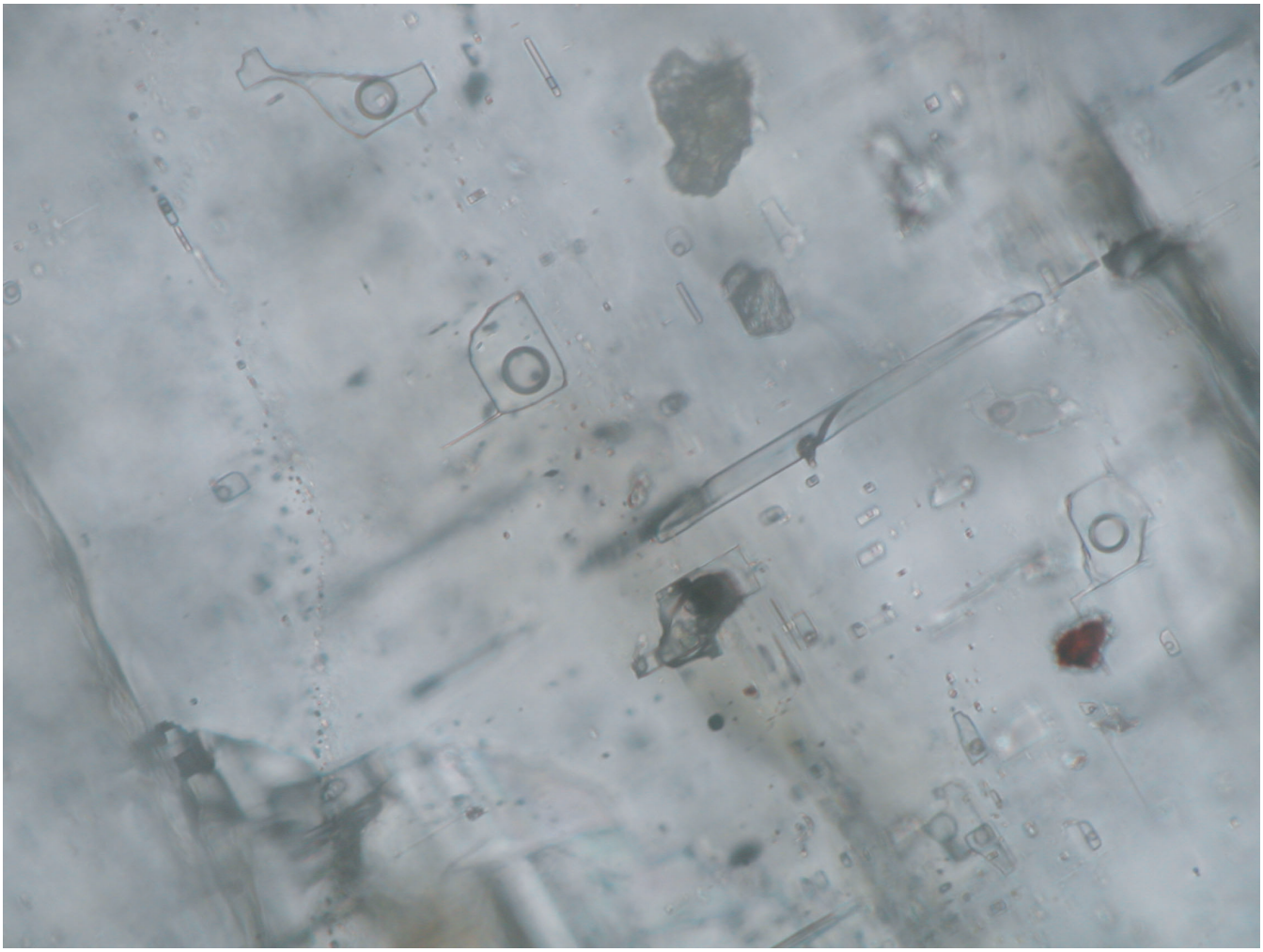

Figure 8. Photomicrograph (plane polarized light) of fluid inclusions in breccia-cementing anhydrite from the depth interval 1170.4-1176.4 m in well M-6B. Large, somewhat rectangular inclusion just northwest of center is about 30 μ in length. These larger inclusions form a three-dimensional array that, however, cannot be ascribed to a growth zone in the host crystal. Thus, the inclusions cannot be considered unambiguously primary in origin.

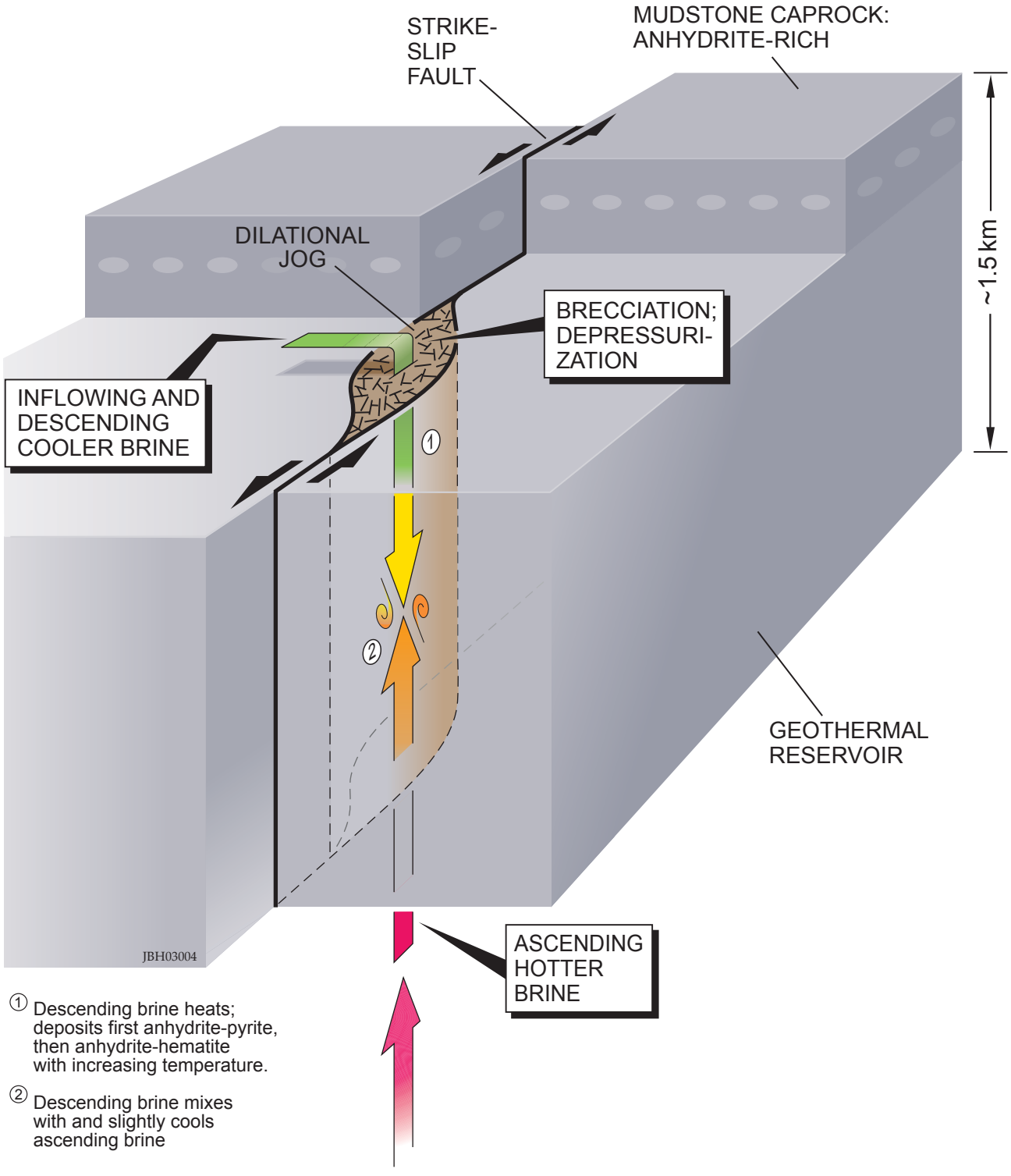

Figure 9. Conceptual diagram illustrating one possible scenario for brecciation, thermal-fluid flow, and mineralization in the hydrothermal system intersected by well M-6B. The governing structure is envisioned to be an antithetic, left-lateral, strike-slip fault in the prevailing, San Andreas-style, right-lateral wrench-fault regime of the Salton trough.

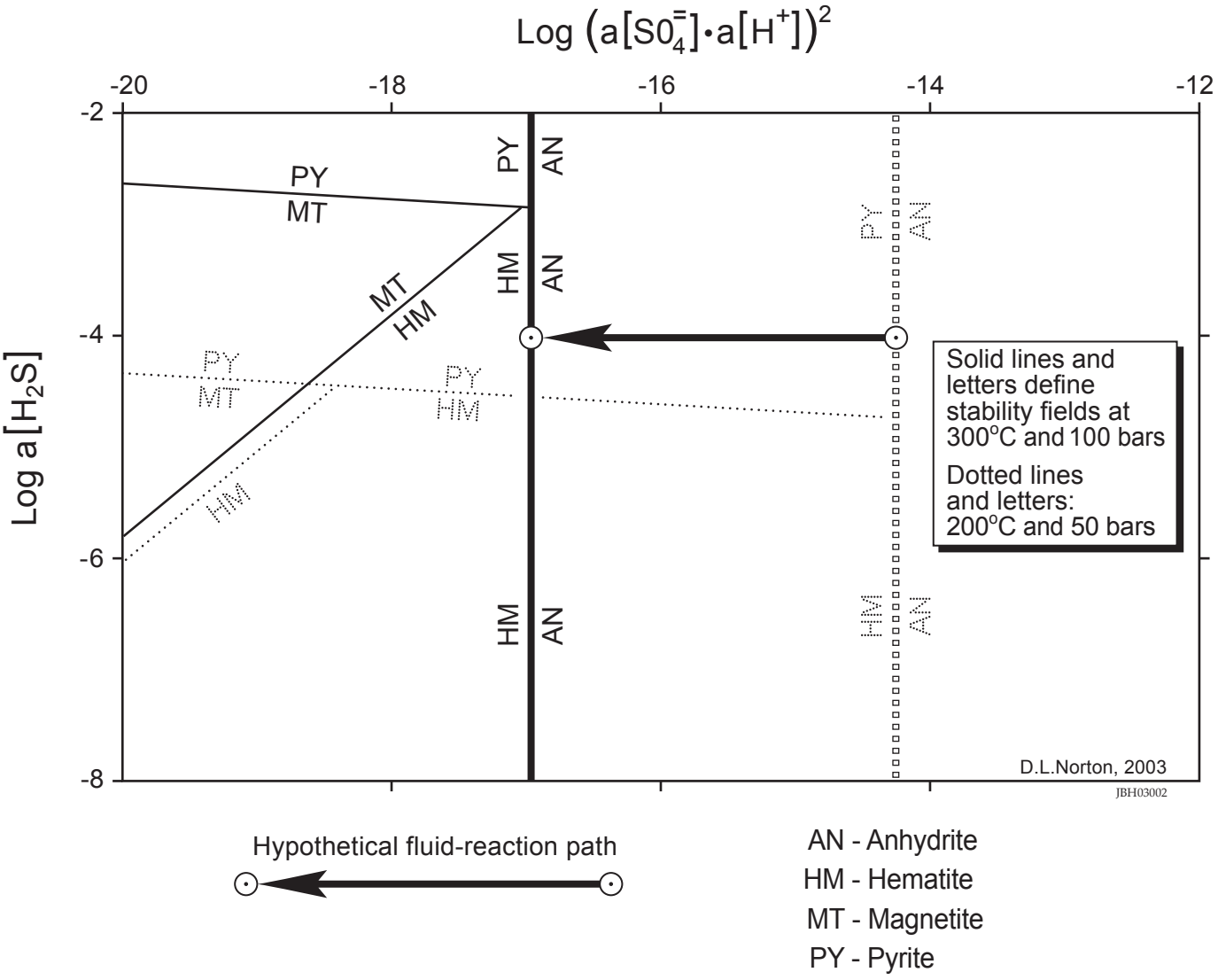

Figure 10. Activity-activity diagram illustrating a fluid-reaction path leading to coprecipitation of specular hematite and anhydrite in dilational breccias of the production zone in well M-6B. Constraints for construction of this diagram are discussed in detail in the text.

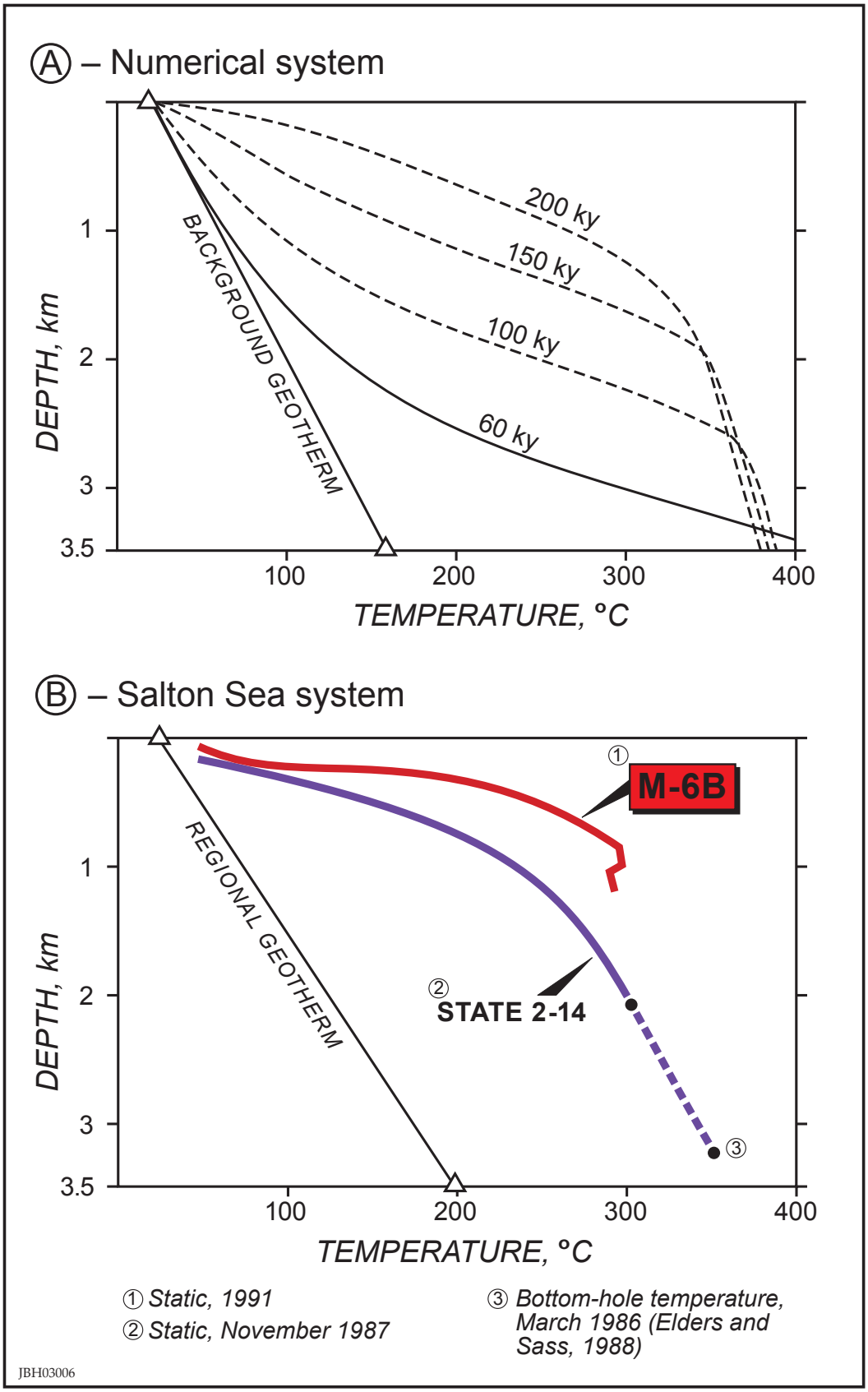

Figure 11. Comparison of computed temperature-depth (T-z) profiles for a highly simplified, generic numeric hydrothermal system (A) with measured static T-z profiles for Salton Sea geothermal wells State 2-14 and M-6B (B). For locations of these wells, please refer to Figure 1. Computations by D.L. Norton using his proprietary Flow-6 software.